The Threshold Photoelectron Spectrum of Cyclobutadiene: Comparison with Time-Dependent Wavepacket Simulations

Lea Bosse,[†] Barry P. Mant,[‡] Domenik Schleier,[†] Marius Gerlach,[†] Ingo Fischer,[*,†] Anke Krueger,[¶] Patrick Hemberger,[§] and Graham Worth[*,‡]

[†]*Institute of Physical and Theoretical Chemistry, University of Wrzburg, D-97074 Wrzburg*

[‡]*Dept. of Chemistry, University College London, 20, Gordon St., London, WC1H 0AJ*

[¶]*Institute of Organic Chemistry, University of Wrzburg, D-97074 Wrzburg*

[§]*Laboratory for Femtochemistry and Synchrotron Radiation, Paul Scherrer Institut (PSI), CH-5232 Villigen*

E-mail: ingo.fischer@uni-wuerzburg.de; g.a.worth@ucl.ac.uk

Phone: +49 (0)931 3186360. Fax: +49 (0)931 31863610

Abstract

The C_4H_4 isomer cyclobutadiene (CBD) is the prime model for antiaromaticity and thus a molecule of considerable interest in chemistry. Since it is highly reactive, it can only be studied under isolated conditions. Its electronic structure is characterized by a pseudo-Jahn-Teller effect in the neutral and a $E \otimes \beta$ Jahn-Teller effect in the cation. As a result, recording photoelectron spectra as well as describing them theoretically has been challenging. Here we present the photoion mass-selected threshold photoelectron spectrum of cyclobutadiene together with a simulation based on time-dependent wavepacket dynamics that includes vibronic coupling in the ion, taking into account eight vibrational modes in the cation. Excellent agreement between theory and experiment is found and the ionization energy is revised to 8.06 ± 0.02 eV.

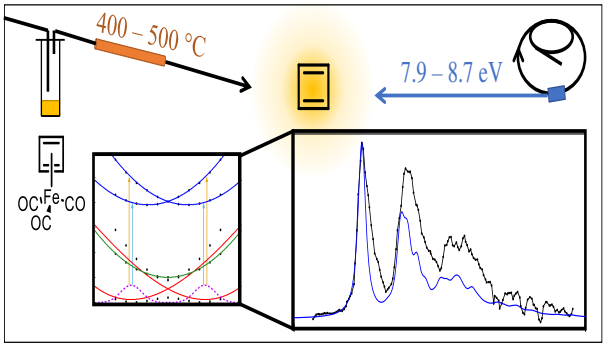

Cyclobutadiene (CBD), C_4H_4 (**1** in Scheme 1) has attracted considerable interest in chemistry as a paradigm for antiaromaticity.[1–4] It is considered to be a biradical with high reactivity[5,6] that can only be studied under isolated conditions. In a simple molecular orbital picture, two electrons would occupy the degenerate e_g antibonding HOMO (highest occupied molecular orbital), leading to a square planar geometry of D_{4h} symmetry and a $^3A_{2g}$ electronic ground state.[7] However, vibronic coupling with a low-lying excited state leads to a pseudo-Jahn-Teller effect and as a result, C_4H_4 exhibits a distorted rectangular D_{2h} symmetry that leads to a singlet ground state of ^1A_g symmetry.[7] The distortion was confirmed after careful evaluation of several IR spectra of matrix-isolated CBD.[8–10] Interestingly, computations suggest that the low-lying excited states S_1, S_2 and T_1 possess D_{4h} symmetry.[7,11]

Traditionally, experimental insight into the electronic structure and the character of molecular orbitals (MO) is obtained from photoelectron spectroscopy.[12] In CBD, ionization leaves a single electron in the e_g orbital and a ^2E_g ionic ground state in D_{4h} symmetry results. As a consequence, this state is subject to a $E \otimes \beta$ Jahn-Teller distortion.[13] Here, vibrational modes of b_{1g} and b_{2g} symmetry lead to a symmetry lowering. Interpretation of the photoelectron spectrum of CBD thus requires inclusion of both, a Jahn-Teller effect in the cation as well as a pseudo-Jahn-Teller effect in the neutral, which leads to a challenging theoretical task. In another antiaromatic biradical, the cyclopentadienyl cation, details of the vibronic coupling were recently unravelled by pulsed field ionisation.[14]

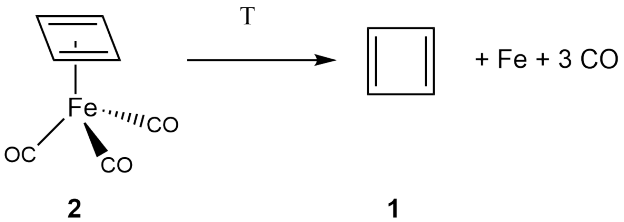

Scheme 1: Cyclobutadiene **1**, is generated by pyrolysis from the Pettit-complex **2**.

Photoelectron spectroscopy of CBD, based on the photolysis or pyrolysis of a suitable precursor thus drew a lot of interest, but the difficulties of generating the molecule cleanly

as well as its high reactivity hampered the experiments. Earlier studies extrapolated an IE of 8.29 eV from the values of related molecules[15] or reported broad bands without assignable vibrational structure, which only permitted the extraction of a band maximum of 8.24 eV.[16] The exception is a 118.2 nm (10.49 eV) photoelectron spectrum of CBD generated by pyrolysis of tricyclopentan-3-one, which was reported by Kohn and Chen (KC).[17] They obtained an adiabatic ionization energy $IE_{ad} = 8.16\,eV$ and resolved a low-frequency vibration at 0.08 eV (650 cm^{-1}). The spectrum was simulated using a rectangular geometry of the ion, as expected from the considerations above and the distorted geometry was confirmed. Furthermore, it was shown that the difference between R_{C-C} and $R_{C=C}$ decreases upon ionization. However, the analysis was based on a harmonic approximation. In 2006, Saddique and Worth presented a simulation of the spectrum, based on wavepacket calculations that used a vibronic coupling model Hamiltonian including corrections up to second order.[18] Only modest agreement was achieved and in particular the 80 meV mode could not be simulated. The reasons for this discrepancy remained unclear.

A potential issue in conventional photoelectron spectroscopy of reactive molecules is the possible perturbation by signals from contaminations. Therefore, we reinvestigated CBD by photoelectron-photoion coincidence spectroscopy (PEPICO), a method that permits to record ion mass-selected (threshold) photoelectron spectra (ms-TPES) for each composition by correlating ions and electrons.[19] A number of reactive molecules generated by pyrolysis[20,21] as well as other methods[22,23] have been studied using PEPICO.

The simulation of the photoelectron spectrum has also been readdressed using wavepacket dynamics simulations and a new vibronic coupling model Hamiltonian[24] (see Mukherjee et al[25] for a recent review on non-adiabatic theory and photoelectron spectra), carefully reparameterized using complete active space with second order perturbation theory (CASPT2) calculations. The agreement between the simulated and measured spectra allows not only confirmation of the rectangular structure, but also an assignment of the vibrations excited during the ionization process.

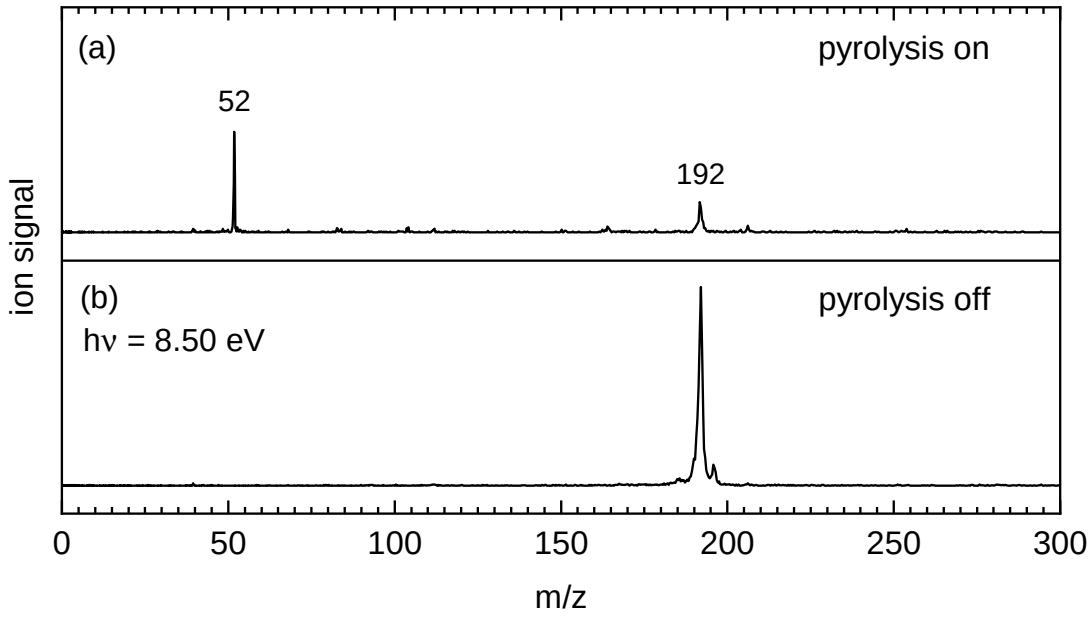

Figure 1: In the photoionization mass spectrum without pyrolysis (b) the precursor signal **2** (m/z 192) dominates. A small peak at m/z 196 is due to $Fe(CO)_5$, a side product formed in the last step of the synthesis. When pyrolysis is turned on (trace (a), intensities scaled by 3), the precursor is converted to C_4H_4 (m/z 52). A photon energy of 8.50 eV was employed for both spectra.

In the present work we generated CBD by pyrolysis from the Pettit-complex **2**, depicted in Scheme 1. This precursor has been employed before in mass spectrometric work on CBD.[26] Figure 1 shows photoionization mass spectra recorded at a photon energy of 8.50 eV. Without pyrolysis (lower trace) only a signal from the precursor **2** is visible, which shows that dissociative photoionization is negligible at this energy. When the pyrolysis is turned on (upper trace), thermal decomposition sets in and a fragment at m/z 52 appears, corresponding to C_4H_4. The best conversion is achieved at a rather low pyrolysis power of 15 W, corresponding to temperatures around 400 - 500 C. Note that CO cannot be ionized at 8.50 eV and is therefore not visible in the spectrum. Interestingly, no signal associated with iron atoms appear, suggesting reactions in the pyrolysis reactor that lead to deposition or formation of species with an IE above 8.50 eV.

The mass-selected threshold photoelectron signal in the m/z 52 mass channel is shown as a black line in Figure 2(a). An intense band at 8.06 eV is assigned to the transition into the rovibronic ground state and thus corresponds to the adiabatic ionization energy IE_{ad} of CBD. It is accurate to within ± 0.02 eV, based on the full width at half maximum of the band. This value is roughly 0.1 eV lower than the previously accepted value by KC, but in excellent agreement with the IE of 8.044 eV computed by CASPT2 in the present work. In addition two broadened bands appear in the spectrum that probably cover several vibrational transitions, the first one appearing at +0.14 eV above the origin. Based on the geometric distortions described above, activity is in particular expected for the ring deformation modes, as well as the C-C and C=C stretching modes.

In addition to the spectrum, simulations are shown based on time-dependent wavepacket dynamics described below. The simulated spectrum in Figure 2(b) is shifted in energy by +15 meV for best agreement with the experiment. To represent the experimental broadening, an exponential damping term was included in the computations, with time constants of 50 fs (blue line in trace (a)) and 150 fs (trace (b)), respectively. This phenomenological damping term takes into account missing terms in the model and experimental line-broadening by

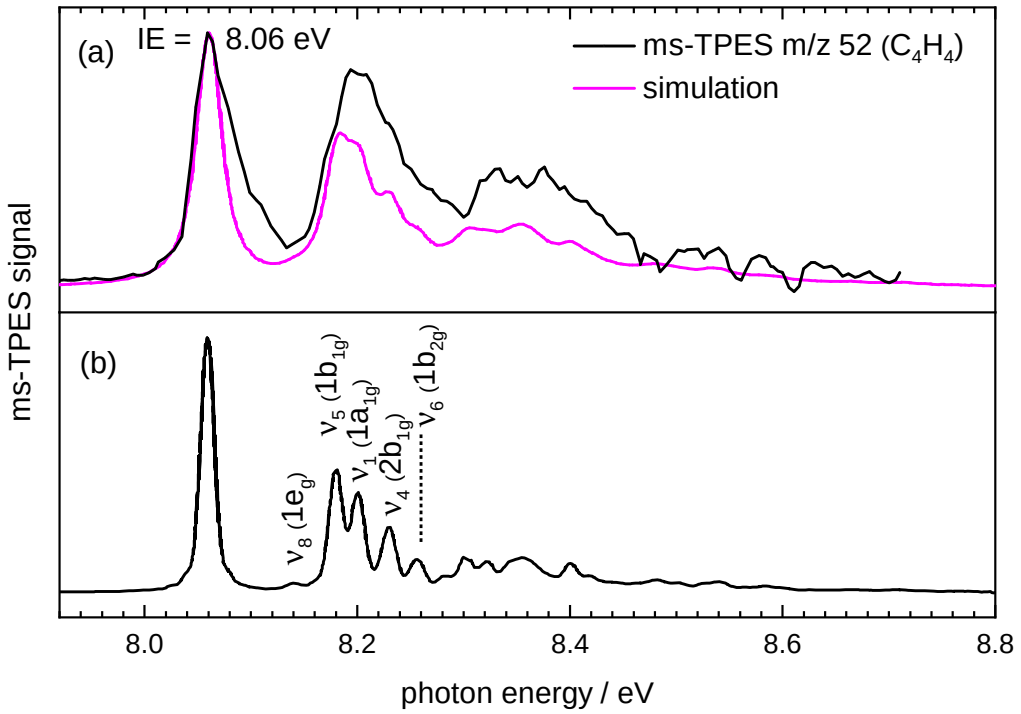

Figure 2: (a) The mass-selected TPE-spectrum (black) yields an IE_{ad} of 8.06 eV. The simulation (see text for details) given as a magenta line provide a very good match to the experimental data. It is based on the simulation given in (b), which shows the vibrational assignment of the fundamental peaks. Note that a damping factor has been added to the simulations to represent the spectral broadening.

convoluting the spectral lines with a Lorentzian function. As can be seen, the agreement is very good and the simulation including a 50 fs damping time fits the shape and position of the vibrational bands. A comparison of the spectrum with a purely adiabatic simulation of Franck-Condon Factors is given in the SI and shows that the first broad band around 8.2 eV is not well represented.

Although the IE_{ad} of 8.06 eV is in agreement with the previous value of 8.16 ± 0.1 eV, the spectra show distinct differences and in particular the previously observed band at +80 meV is absent in Figure 2(a). To rationalize these differences, we considered possible explanations. First, other isomers of m/z 52 might be carriers of bands in either spectrum. In particular methylenecyclopropene ($IE_{exp} = 8.15$ eV)[27] and tetrahedrane ($IE_{calc} = 8.06$ eV) have IE's in the same range. The former has been studied before[27] and its spectrum does neither resemble the one given in Figure 2 nor the one reported by KC and can thus be ruled out. Tetrahedrane on the other hand is highly unstable and expected to isomerize at elevated temperatures. Furthermore, a Franck-Condon simulation resulted in a different spectrum. A second consideration is based on the fact that the two experiments differ in the choice of precursor. While we employed the complex **2**, KC utilized tricyclopentan-3-one (C_5H_4O) as a precursor, so its isomers have to be included in the analysis as well. In fact, for the open chain isomer $CH_2CCHCHCO$ we compute $IE_{calc} = 8.16$ eV, which is close to the IE of CBD. The +80 meV band observed by KC might thus be assigned to the IE of this precursor isomer. The deviation between the conventional PES and the earlier simulations could thus be traced back to a pyrolysis side product, which causes the appearance of an additional band. A third possible explanation would be an accidental autoionizing resonance at 10.49 eV, which artificially enhances the $\nu_8(e_g)$ mode in the earlier spectrum.

The agreement between the simulated and experimental spectra enables an assignment of the peaks in the spectrum, shown in Figure 2(b). The model, based on *ab initio* data, concludes that the dynamical behaviour of both the neutral and cationic CBD is dominated by the vibration, $\nu_4(b_{1g})$, that takes the structure between two rectangular mimina with

symmetry D_{2h} via a square transition state with D_{4h} symmetry. This vibration is, however, strongly coupled to the $\nu_1(a_{1g})$ and $\nu_5(b_{1g})$ vibrations (vibrations shown in Figure 3(c) - note the molecule is oriented in the xy plane with the axes bisecting the C–C bonds). As a result the three peaks assigned to these modes are actually mixed modes with the assignment made according to the nearest zero-order frequency. The importance of the ν_4 mode is seen in that a simulation with only the ν_1 or ν_5 vibration results in either no peaks (except the 0-0 peak) or a single very small peak, respectively. Adding the ν_4 vibration results in the band observed. The $\nu_6(b_{2g})$ mode also becomes active due to the Jahn-Teller coupling, resulting in a weak peak. An analysis of the composition of the peaks is made in the supporting information Section S5.

Slices through the potential energy surfaces for CBD along the ν_4 vibrational coordinate are sketched in Figure 3. The lowering of symmetry from D_{4h} to D_{2h} in the CBD neutral is due to pseudo-Jahn-Teller coupling of the $^1B_{1g}$ ground state at D_{4h} with a low-lying $^1A_{1g}$ excited-state predicted by the CASPT2 calculations to lie at 2.03 eV. A second low-lying excited-state of B_{2g} symmetry is also predicted to be nearly degenerate with the A_{1g} state. The transition barrier for the D_{4h} to D_{2h} deformation is 0.41 eV in height, measured from the global minimum, in good agreement with recent calculations.[28] At the CASPT2/6-311G** level of theory, the C–C and C–H bond lengths of the D_{4h} TS are 1.45 Å and 1.08 Å. At the D_{2h} minimum the C–H bonds are still 1.09 Å, but the C–C bonds are now 1.36 Å and 1.56 Å, respectively.

The cation ground states are described by an E$\otimes\beta$ Jahn-Teller interaction, with the doubly degenerate ^2E_g electronic state at D_{4h} lowered in symmetry by vibrations of b_{1g} and b_{2g} symmetry, hence the excitation of the b_{1g} vibrations seen in the spectrum. Again the $\nu_4(b_{1g})$ vibration provides the strongest coupling. The minimum energy structure of the cation is again D_{2h}, but it has contracted from the neutral structure: the C–C bond lengths are 1.39 Å and 1.51 Å, and the C–H 1.08 Å.

In conclusion, excellent agreement between the threshold photoelectron spectrum of cy-

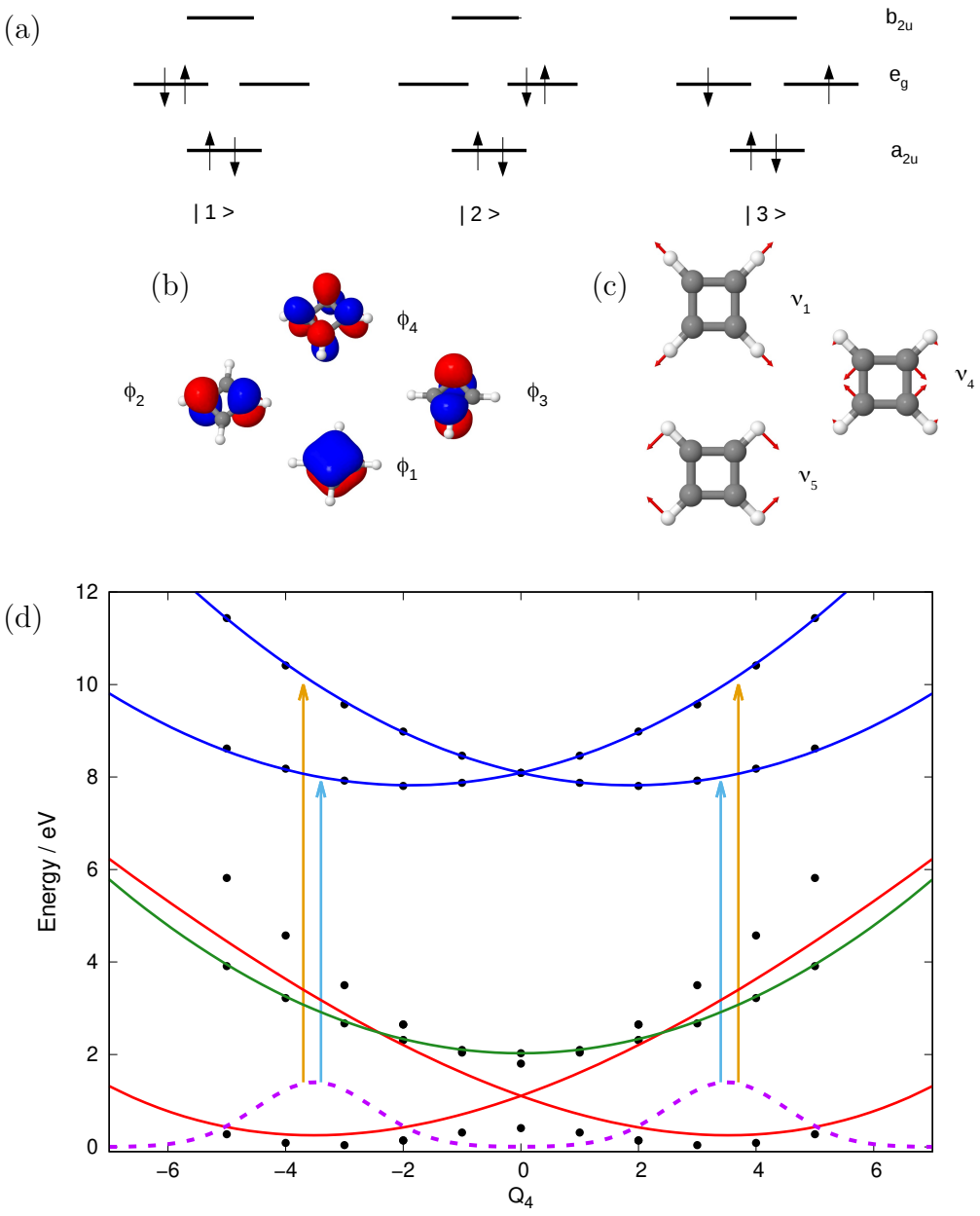

Figure 3: (a) Configurations of neutral CBD involving the four π-MOs, (b) Representation of the CBD π-MOs (c) Main three vibrations of neutral CBD at the D_{4h} TS (d) Slices through the CBD potential energy surface along the ν_4 vibrational coordinate and wave packet excitation from neutral to cation along the ν_4 vibrational coordinate. Relaxed wave packet (purple dashed line), diabatic representation of neutral CBD ground states $|1\rangle$ and $|2\rangle$ from mixing $|\tilde{X}(^1B_{1g})\rangle$ and $|\tilde{A}(^1A_{1g})\rangle$ adiabatic states (red lines), excited neutral state $|3\rangle = |\tilde{B}(^1B_{2g})\rangle$ (green line), degenerate ^{2}E$_g$ cation states (blue lines), adiabatic CASPT2 energies (black dots). $Q_4 = 0$ is the D_{4h} point.

clobutadiene, C_4H_4 and a time-dependent wavepacket dynamics simulation has been achieved and the ionization energy is revised to 8.06 ± 0.02 eV. The simulations allow an analysis of the spectrum and show that the key feature is three strongly coupled vibrational modes that form the main peaks. After decades of research, the photoelectron spectrum of C_4H_4, one of the archetypical antiaromatic molecule, is finally resolved.

Methods

The Pettit-complex **2** was synthesized by optimising an earlier route reported by Pettit *et al.*[29,30] The details of the procedure, the modifications and the analytical data for the intermediate steps are described in the supporting information. The liquid precursor was put in a sample container, seeded in Ar and expanded through a 100 m orifice into an electrically heated SiC tube based on an earlier design.[31] Here cyclobutadiene **1**, was generated by a thermal dissociation.

TPE-spectra were recorded at the VUV beamline of the Swiss Light Source (SLS) at the Paul-Scherrer Institute, Villigen/CH.[32] Synchrotron radiation is provided by a bending magnet. It is collimated and diffracted by a plane grating (150 grooves*mm^{-1}) with a resolving power of 10^4. Higher harmonic radiation is suppressed in a rare gas filter operated with a Kr/Ar/Ne mixture at a pressure of 10 mbar. The photon energy was scanned in 5 meV steps and calibrated using autoionization resonances in Ar in both first and second order of the grating. Experiments were carried out in a free jet apparatus equipped with a time-of-flight mass spectrometer and a velocity map imaging photoelectron spectrometer.[22] Ions and electrons were collected in coincidence, permitting to record ion mass-selected photoelectron spectra. Threshold electrons were selected with an energy resolution of 3 - 5 meV and the contribution of background electrons was subtracted following the procedure given in Ref.[33]

Ionization energies of the various isomers of (C_4H_4) and (C_5H_4O) were computed by the G4 composite methods, using the Gaussian 09 suite of programs.[34] The photoelectron spec-

trum was simulated using time-dependent wavepacket dynamics using the MCTDH method[35] as implemented in Quantics.[36]

For both the neutral and the cation, a vibronic coupling Hamiltonian model[24] was employed. The diabatic potentials are expressed, through a Taylor series, in terms of dimensionless (mass-frequency scaled) normal modes Q_α around a particular point, $\mathbf{Q}_0$, here taken as the $D_{4\mathrm{h}}$ TS geometry. The Hamiltonians can therefore be written in matrix form as

$$\mathbf{H} = \mathbf{H}^{(0)} + \mathbf{W}^{(0)} + \mathbf{W}^{(1)} + \ldots \tag{1}$$

The Hamiltonian parameters were obtained by least squares fitting to CASPT2 (4,4)/6-311G* calculations carried out using Molpro.[37–39]

The zero-order Hamiltonian $\mathbf{H}^{(0)}$ is based on the harmonic approximation to the neutral CBD ground-state, with excitation and ionization energies at D_{4h}

$$H_{ii}^{(0)} = E_i + \sum_\alpha \frac{\omega_\alpha}{2}\left(\frac{\partial}{\partial Q_\alpha^2} + Q_\alpha^2\right) \tag{2}$$

The absolute value of the imaginary frequency for mode Q_4 is used for the coordinate definition. For some modes, including Q_4 the harmonic potential is substituted by state-specific Morse potentials for better fits. The subsequent matrices include the effects of electronic excitation and vibronic coupling as a Taylor expansion around the point $\mathbf{Q}_0$. The key cut through the potentials, along the $Q_4(b_{1g})$ vibration that takes the molecule from D_{4h} to D_{2h} symmetry, is shown in Figure 3(d).

Neutral CBD has 2 electrons in the doubly degenerate HOMO, resulting in the three configurations, shown symbolically in Figure 3(a) with the MOs in 3(b). The adiabatic states were taken as the symmetry adapted combinations of the diabatic states related to these configurations, i.e. $|\tilde{X}(^1B_{1g})\rangle = |1\rangle + |2\rangle$, $|\tilde{A}(^1A_{1g})\rangle = |1\rangle - |2\rangle$ and $|\tilde{B}(^1B_{2g})\rangle = |3\rangle$. At D_{4h}, the diabatic states $|1\rangle$ and $|2\rangle$ are degenerate with a constant coupling. This is seen in Figure 3(d) where the diabatic potentials for states $|1\rangle$ and $|2\rangle$ are the red lines, degenerate

at D_{4h}, but equivalent to the $\tilde{X}, \tilde{A}$ adiabatic energies of the ground- and first-excited states given by the dots. For all other states, the adiabatic and diabatic states are identical at $\mathbf{Q}_0$.

The ground state nuclear wavefunction of neutral CBD was obtained using energy relaxation[35] of an initial eight-mode wavepacket built from harmonic oscillator eigenfunctions. A vertical excitation was then performed by placing the ground state neutral wavefunction from state $|1>$, which is localized in one D_{2h} minimum, on one of the cation $^2\mathrm{E_g}$ electronic states, as shown schematically in Figure 3. For the first band in the photoelectron spectrum studied here the excitation was to the ground-state of the cation. The wavepacket was then propagated on this state for 150 fs. The photoelectron spectrum was obtained from the Fourier transform of the autocorrelation function as

$$I(\omega) \propto \omega \int_{-\infty}^{\infty} \mathrm{d}t\, C(t) e^{i\omega t} e^{(-t/\tau)}, \tag{3}$$

where the last factor is an exponential dampening term to simulate experimental broadening in the photoelectron spectra and the autocorrelation function C(t) is defined as

$$C(t) = \langle \Psi(0) | \Psi(t) \rangle = \left\langle \Psi\left(\frac{t}{2}\right)^* \middle| \Psi\left(\frac{t}{2}\right) \right\rangle. \tag{4}$$

Further details of the model and dynamics calculations, with all the parameters, are in the supporting information.

Acknowledgement

The experiments were performed at the VUV beamline of the Swiss Light Source, located at the Paul Scherrer Institute (PSI). The work was financially supported by the Deutsche Forschungsgemeinschaft, research training school GRK 2112 (Molecular Biradicals) as well as Fi 575/13-2. It was also supported by the Swiss Federal Office for Energy (BFE Contract Number SI/501269-01) and by the Laboratory for Thermal Processes and Combustion (LTV)

located at PSI.

Supporting Information Available

A description of the synthesis of the Pettit-complex **2**, including analytical data as well as full details of the *ab initio* calculations, vibronic coupling Hamiltonian models and parameters and MCTDH calculations are given in the supporting information.

References

(1) Judy, I.; Wu, C.; Mo, Y.; Evangelista, F. A.; von Ragué Schleyer, P. *Chem. Comm.* **2012**, *48*, 8437–8439.

(2) Bally, T. *Angew. Chem. Int. Ed.* **2006**, *45*, 6616–6619.

(3) Allen, A. D.; Tidwell, T. T. *Chem. Rev.* **2001**, *101*, 1333–1348.

(4) Maier, G. *Angew. Chem.* **1974**, *86*, 491–505.

(5) Abe, M. *Chem. Rev.* **2013**, *113*, 7011–7088.

(6) Stuyver, T.; Chen, B.; Zeng, T.; Geerlings, P.; De Proft, F.; Hoffmann, R. *Chem. Rev.* **2019**, *119*, 11291–11351.

(7) Nakamura, K.; Osamura, Y.; Iwata, S. *Chem. Phys.* **1989**, *136*, 67–77.

(8) Masamune, S.; Souto-Bachiller, F. A.; Machiguchi, T.; Bertie, J. E. *J. Am. Chem. Soc.* **1978**, *100*, 4889–4891.

(9) Bally, T.; Masamune, S. *Tetrahedron* **1980**, *36*, 343–370.

(10) Maier, G. *Angew. Chem.* **1988**, *100*, 317–341.

(11) Karadakov, P. B. *J. Phys. Chem. A* **2008**, *112*, 7303–7309.

(12) Eland, J. H. D. *Photoelectron Spectroscopy*; Butterworths, London, 2013.

(13) Paterson, M.; Bearpark, M.; Robb, M.; Blancafort, L.; Worth, G. *Phys. Chem. Chem. Phys.* **2005**, *7*, 2100–2115.

(14) Wörner, H. J.; Merkt, F. *J. Chem. Phys* **2007**, *127*, 034303.

(15) Worley, S.; Webb, T.; Gibson, D. H.; Ong, T.-S. *J. Organomet. Chem.* **1979**, *168*, C16–C20.

(16) Kreile, J.; Mnzel, N.; Schweig, A.; Specht, H. *Chem. Phys. Lett.* **1986**, *124*, 140–146.

(17) Kohn, D. W.; Chen, P. *J. Am. Chem. Soc.* **1993**, *115*, 2844–2848.

(18) Saddique, S.; Worth, G. *Chem. Phys.* **2006**, *329*, 99–108.

(19) Baer, T.; Tuckett, R. P. *Phys. Chem. Chem. Phys.* **2017**, *19*, 9698–9723.

(20) Schßler, T.; Deyerl, H.-J.; Dmmler, S.; Fischer, I.; Alcaraz, C.; Elhanine, M. *J. Chem. Phys.* **2003**, *118*, 9077–9080.

(21) Reusch, E.; Holzmeier, F.; Constantinidis, P.; Hemberger, P.; Fischer, I. *Angew. Chem. Int. Ed.* **2017**, *56*, 8000–8003.

(22) Sztaray, B.; Voronova, K.; Torma, K. G.; Covert, K. J.; Bodi, A.; Hemberger, P.; Gerber, T.; Osborn, D. L. *J. Chem. Phys.* **2017**, *147*, 013944.

(23) Garcia, G. A.; Gans, B.; Krger, J.; Holzmeier, F.; Rder, A.; Lopes, A.; Fittschen, C.; Alcaraz, C.; Loison, J. C. *Phys. Chem. Chem. Phys.* **2018**, *20*, 8707–8718.

(24) Köppel, H.; Domcke, W.; Cederbaum, L. S. *Adv. Chem. Phys.* **1984**, *57*, 59.

(25) Mukherjee, B.; Naskar, K.; Mukherjee, S.; Ghosh, S.; Sahoo, T.; Adhikari, S. *Int. Rev. Phys. Chem.* **2019**, *38*, 287–341.

(26) Li, P. H.; McGee, H. A. *Journal of the Chemical Society D: Chemical Communications* **1969**, 592–593.

(27) Staley, S. W.; Norden, T. W. *J. Am. Chem. Soc.* **1989**, *11*, 445–449.

(28) Varrasa, P. C.; Gritzapisb, P. S. *Chem. Phys. Lett* **2018**, *711*, 166–172.

(29) Pettit, R.; Henery, J. *Org. Synth.* **2003**, *50*, 36.

(30) Pettit, R.; Henery, J. *Org. Synth.* **2003**, *50*, 21.

(31) Kohn, D. W.; Clauberg, H.; Chen, P. *Rev. Sci. Instrum.* **1992**, *63*, 4003–4005.

(32) Johnson, M.; Bodi, A.; Schulz, L.; Gerber, T. *Nucl. Instrum. Meth. A* **2009**, *610*, 597–603.

(33) Sztaray, B.; Baer, T. *Rev. Sci. Instrum.* **2003**, *74*, 3763–3768.

(34) Frisch, M. J. et al. Gaussian 09, Revision E.01. 2013; Gaussian Inc. Wallingford CT.

(35) Beck, M. H.; Jäckle, A.; Worth, G. A.; Meyer, H.-D. *Phys. Rep.* **2000**, *324*, 1–105.

(36) Worth, G. A. *Comput. Phys. Commun.* **2020**, *248*, 107040.

(37) Werner, H.-J.; Knowles, P. J.; Knizia, G.; Manby, F. R.; Schütz, M. *WIREs Comput. Mol. Sci.* **2012**, *2*, 242–253.

(38) others,, et al. **2019**, see https://www.molpro.net.

(39) Werner, H.-J. et al. *J. Chem. Phys.* **2020**, *152*, 144107.

Graphical TOC Entry

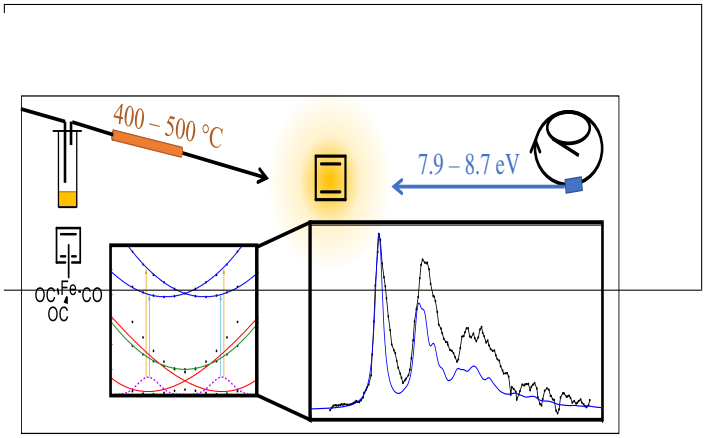

The surrounding frame is 9 cm by 3.5 cm, which is the maximum permitted for *Journal of the American Chemical Society* graphical table of content entries. The box will not resize if the content is too big: instead it will overflow the edge of the box.
This box and the associated title will always be printed on a separate page at the end of the document.